analytical chemistry

Article

Cite This: Anal. Chem. 2018, 90, 11917−11924

pubs.acs.org/ac

Analysis of Electrochemically Elusive Trace Metals with Carbon Fiber Microelectrodes

Thushani Siriwardhane, Yangguang Ou, Pavithra Pathirathna, and Parastoo Hashemi*

Department of Chemistry and Biochemistry, University of South Carolina, 631 Sumter Street, Columbia, South Carolina 29208, United States

ABSTRACT: There is great interest in rapidly monitoring metals of biological and environmental interest. Electrochemistry is traditionally a powerful tool for metal analysis but can be limited by its scope and low temporal resolution. The scope is limited by the potential window of the working electrode and rapid analysis is limited, in part, by the need for nucleation/growth for preconcentration. In prior work, we showed that a rapid equilibrium mediated preconcentration process facilitated fast scan cyclic voltammetry (FSCV) responses to Cu(II) and Pb(II) at carbon fiber microelectrodes (CFMs). In this manuscript, we apply this same principle to Ca(II), Al(III), Mg(II), and Zn(II), metal ions that are traditionally difficult to electroanalyze. We demonstrate FSCV reduction peaks for these four metals whose positions and amplitudes are dependent on adsorption. The adsorption profiles of these ions onto CFMs follow Langmuir's theory for monolayer coverage. We calculate the thermodynamic equilibrium constant of metal adsorption onto CFMs and find that these constants follow the same order as those previously reported by other groups on other activated carbon materials. Finally, a real-time complexation study is performed with ligands that have preference for divalent or multivalent ions to probe the selectivity of the real-time signal. We observe a linear relationship between formation constant (k_f) and % change in the FSCV signal and use this correlation to, for the first time, report the k_f of an Al(III)-complex. This work demonstrates the versatility of FSCV as a method with capacity to extend the scope of rapid electroanalysis.

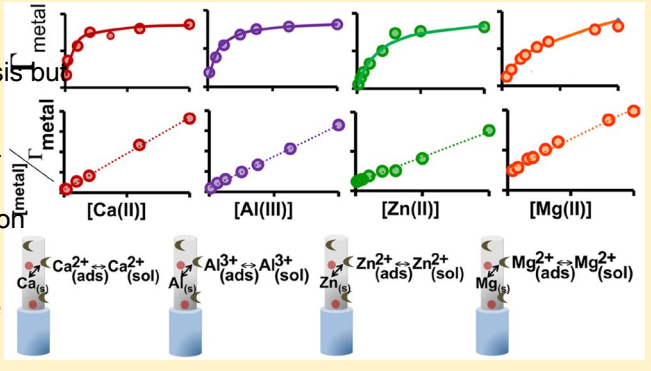

Real-time metal analysis is useful for a variety of laboratory and real world situations.[1−3] Electrochemistry is well suited for metal measurements because cations can be electrostatically preconcentrated onto traditional electrode materials for high sensitivity measurements. However, the scope of metals that can be analyzed with traditional electrochemistry is limited to those whose redox potentials fall within the potential window of the working electrode. As such, direct electroanalysis of species with highly negative reduction potentials, such as Ca(II), Al(III), and Mg(II), which are analytes of biological and environmental interest, is challenging.[4,5] Previous electrochemical analysis of these species has been via complexation strategies,[6−8] which are lengthy and laborious and thus highly limit in situ, real-time analysis. Additionally, for metals that can be electroanalyzed within the potential window of the working electrode, nucleation and growth processes underpin the electrochemical response. In the case of Zn(II), another significant ion of interest, this phenomenon necessitates an activation procedure on solid electrodes that provide small amounts of zinc to act as nucleation sites.[9] Taken together, the activation and proceeding nucleation and growth processes prevent fast analysis, in addition to compromising stability due to Zn build up over time. While nucleation and growth are largely stabilized using Hg and Bi,[10] this does not much improve temporal resolution since minutes or tens of minutes are still required for preconcentration of metal ions into the Hg amalgam or Bi fused alloy. Furthermore, limited potential window remains problematic, along with toxicity and practicality concerns (in the case of Hg). There is, thus, a clear need for new materials and methods that enable rapid analysis of metals such as those described above.

In recent years, we have been employing fast scan cyclic voltammetry (FSCV) at carbon fiber microelectrodes (CFMs) for sub second analysis of Cu(II) and Pb(II).[11,12] This method is sensitive and fast because the signal is driven by rapid preconcentration via adsorption of positive ions, rather than nucleation/growth, onto activated carbon electrodes. We previously studied the carbon fiber-metal adsorption thermodynamic equilibrium and found that this equilibrium facilitates redox processes such that cyclic voltammograms (CVs) for Cu(II) and Pb(II)[13] could be obtained at high scan rates. In this work, we seek to establish whether this principle can be applied to metals that are traditionally difficult to electrochemically analyze.

Received: May 17, 2018
Accepted: August 28, 2018
Published: August 28, 2018

DOI: 10.1021/acs.analchem.8b02210
Anal. Chem. 2018, 90, 11917−11924

We observe, for the first time, FSCV reduction peaks within the CFM potential window for Ca(II), Al(III), Mg(II) and Zn(II). We demonstrate that the position and amplitude of redox peaks obtained for these species depend on scan rate. The adsorption profiles of these metals using fast scan controlled-adsorption voltammetry (FSCAV) show that the adsorption follows a Langmuir monolayer isotherm. The thermodynamic equilibrium constant of adsorption on CFMs is calculated for each metal and we find that these adsorption constants follow the same order as previously reported by other groups on other activated carbon materials. Finally, we perform a real-time complexation study using 1,2-bis(o-aminophenoxy)ethane-N,N,N′,N′-tetraacetic acid (BAPTA) and ethylen-diaminetetra-acetic acid (EDTA), which preferentially bind divalent and multivalent cations, respectively,[14−16] to address selectivity of the rapid response. Lastly, we use a linear relationship between formation constant (k_f) and % change in concentration after ligand addition to determine the k_f of Al(III)-BAPTA complexation. This study highlights FSCV as a fast and versatile electrochemical tool whose analytical scope reaches beyond traditional methods.

EXPERIMENTAL SECTION

Solutions. Unless otherwise stated, all chemicals were purchased from Sigma-Aldrich (St. Louis, MO). A 0.01 M sodium chloride (NaCl) solution (certified ACS) was used as the background electrolyte. Ca(II), Al(III), Zn(II), and Mg(II) solutions were made by dissolving $Ca(NO_3)_2$ (certified ACS), $Al(NO_3)_3$ (ACS reagent, ≥98%), $Zn(NO_3)_2$ (reagent grade, 98%), $Mg(NO_3)_2$ (ACS reagent grade, 99%) in 0.01 M NaCl, respectively. Both ligands, EDTA (anhydrous, ≥99%) and BAPTA (≥98%), were prepared using the same concentration NaCl solution. The solution's pH was 5.84 ± 0.05 (standard deviation). This is the ambient pH of the 0.01 M NaCl solution; while redox peak positions depend on pH, these peaks are apparent over a rather wide pH range. The following concentrations are for real-time complexation studies. 2 mM Mg(II) solution was injected into solutions with 1 mM BAPTA or EDTA (Figure 6B); 10 μM Al(III) was injected into solutions with either 5 μM BAPTA or 5 μM EDTA (Figure 6C). In total, 20 μM Zn(II) was injected into solutions with either 10 μM BAPTA or 10 μM EDTA (Figure 6D). $ZnSO_4$ (bioreagent grade, suitable for cell culture) was used to test whether or not there was an effect of the anion on the current during flow injection analyses. All solutions were made in deionized water.

Microelectrodes. CFMs were prepared as described elsewhere.[11] Briefly, using vacuum suction, a carbon fiber (5 μm radius, T-650, Cytec Industries, NJ) was inserted into a glass capillary (1.0 mm external diameter, 0.5 internal diameter, A-M systems, Inc., Sequim, WA). A vertical micropipet puller (Narishige, Tokyo, Japan) was used to pull the fiber-filled capillary, creating a carbon-glass seal. Under an optical microscope, the electrode was cut to 150 μm. The electrodes were cycled for 10 min at 60 Hz and 10 min at 10 Hz using the dopamine waveform first to activate and clean the surface, with the exception of Mg(II). Figure 1 summarizes the different optimized waveforms for each metal of interest and these were applied after the initial cycling. Scan rates varied per experiment and were defined in figure captions.

Cyclic Voltammetry. A 2-electrode system was employed for slow-scan and fast scan cyclic voltammetry. For slow-scan cyclic voltammetry (scan rates ≤100 $V\,s^{-1}$), a microelectrode was placed into a continuously stirred solution of metal nitrate dissolved in 0.01 M NaCl. A triangular waveform was applied using custom build software, Wildcat CV, written in LAB-VIEW 2014 (National Instruments, Austin, TX). Only solutions for slow-scan cyclic voltammetry were nitrogen-purged prior to experimentation. The Ag/AgCl reference electrode was fabricated by electroplating Cl onto a Ag wire (A-M systems, WA). FSCV experiments (scan rates ≥50 $V\,s^{-1}$) were conducted with a potentiostat (Dagan Corporation, Minneapolis, MN) and custom-built integration unit that incorporated data acquisition cards.

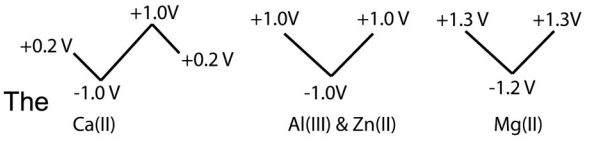

Figure 1. Optimized waveforms for the different metals.

Fast Scan Controlled-Adsorption Voltammetry (FSCAV). FSCAV experiments were consistent with previous reports.[17,18] An electronic relay (ADG-419, Analog Device) was used to switch between the waveform at 100 Hz and a constant potential (resting potential). The delay time for the adsorption of metals onto the CFM was 10 s. Data analysis of the buffer-subtracted response curve (current vs voltage) was performed with LabVIEW 2014 software by integrating the reduction peak from the background subtracted CVs of metals. The surface coverage (Γ_{metal}) was calculated using Faraday's law, summarized by $\Gamma_{metal} = Q/(nFA)$, where Q is the charge obtained from integrating FSCAV peaks, n is the number of electrons, and A is the surface area.[19] Since Ca(II), Al(III), Zn(II), and Mg(II) followed monolayer adsorption, a linearized Langmuir isotherm (eq 1) was used to fit the data such that C is the concentration of metal in the bulk solution, and Γ_{max} is the maximum monolayer coverage at CFM.

$$\frac{C}{\Gamma_{metal}} = \frac{1}{\Gamma_{max}}C + \frac{1}{\Gamma_{max}K} \quad (1)$$

K is the forward equilibrium constant for the following process,

$$\text{adsorbate} + \text{adsorbent} \rightleftharpoons \text{adsorption complex}$$

such that

$$K = \frac{[\text{adsorption complex}]}{[\text{adsorbate}][\text{adsorbent}]} \quad (2)$$

with unit of $cm^3\,mol^{-1}$. However, because the concentration of the carbon fiber ([adsorbent]) does not change, we assumed an activity of unity. Thus, eq 2 can be simplified to

$$K_{ads} = \frac{[\text{adsorbed species}]}{[\text{adsorbate}]} \quad (3)$$

where K_{ads} is unitless and this is the equilibrium constant we report in this manuscript.

Data Analysis. Custom software (WCCV 3.06, written in LABVIEW 2014 by Knowmad Technologies, LLC, Tucson, AZ) was employed to collect and analyze data using background subtraction, signal averaging, and digital filtering. Data was background-subtracted and filtered using a fourth order Butterworth low pass filter. The CVs were stacked in time to produce a 2-D color plot, in which the x-axis is time, y-axis is potential applied, and the color indicates current. Cyclic voltammograms were extracted from the software as text files and imported into Excel for further analysis.

DOI: 10.1021/acs.analchem.8b02210
Anal. Chem. 2018, 90, 11917−11924

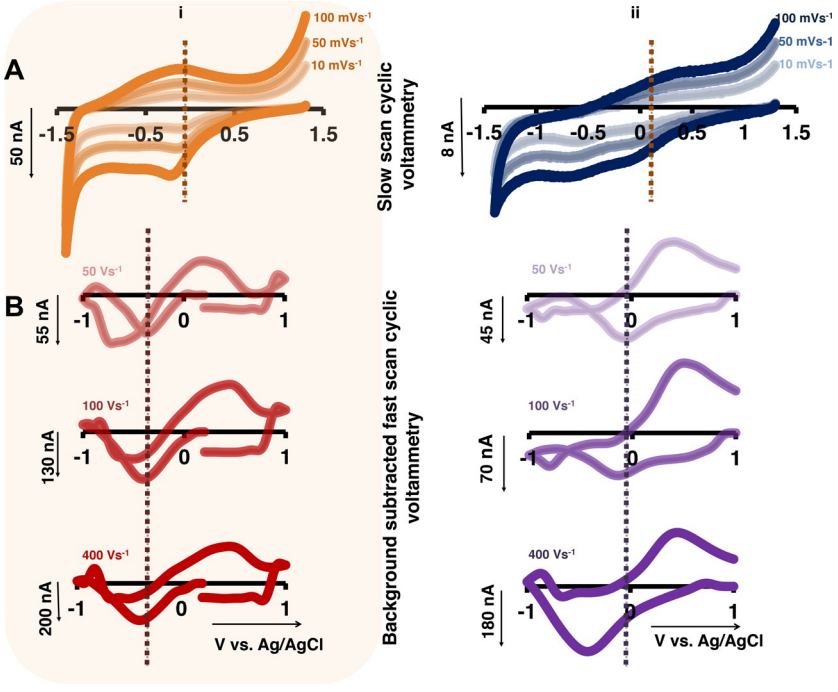

Figure 2. CVs collected for 1.0 M Ca(II) (left column, orange and red) and 0.1 M Al(III) (right column, blue and purple) with increasing scan rat (A) slow (10−100 mV s^{-1}) and (B) fast scan rates (50−400 V s^{-1}).

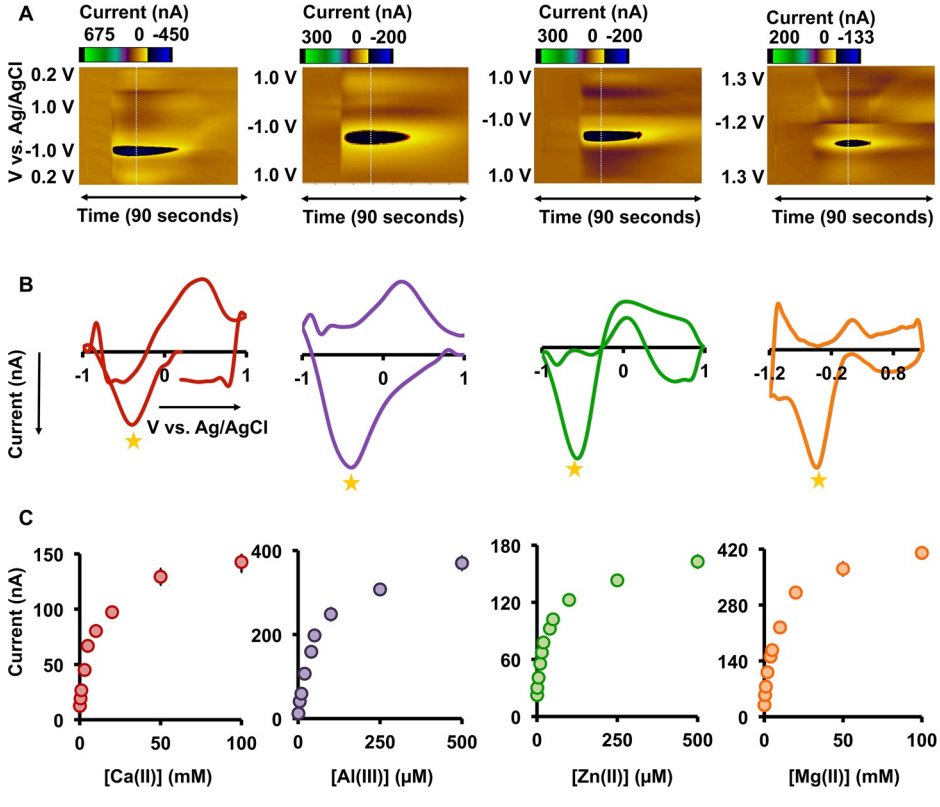

Figure 3. FSCV characterization for Ca(II) (red), Al(III) (purple), Zn(II) (green), and Mg(II) (orange). (A) Representative color plots for each metal. 90 s total data acquisition time with 30 s injection time. (B) Representative CVs at 200, 300, 400, and 200 V s^{-1}, respectively, for 100 mM, 20 μM, 20 μM, and 1 mM concentrations of Ca(II), Al(III), Zn(II), and Mg(II). (C) Calibration curves constructed for each metal.

RESULTS AND DISCUSSION

Redox Peaks for Ca(II) and Al(III) on CFMs. It is not possible to voltammetrically analyze species whose redox potential falls outside the potential window of the electrode substrate. A number of important metals, including Ca(II) and Al(III), are considered challenging to electroanalyze with traditional electrode materials due to this constraint.

DOI: 10.1021/acs.analchem.8b02210
Anal. Chem. 2018, 90, 11917−11924

We previously determined that the adsorption of Cu(II) onto CFMs enables a thermodynamically favorable preconcentration equilibrium that underlies the rapidity of the FSCV signal.[13] During a slow scan cyclic voltammogram (CV) of Cu(II), we observed classical nucleation/growth and stripping peaks. Interesting we observed an additional redox couple. When the scan rate was increased, the nucleation/growth peaks decreased in amplitude while the additional peaks increased in amplitude and subsequently turned into the classical FSCV Cu(II) response. By taking atomic force microscopy images at different points of the slow-scan experiment, we observed solid Cu deposition after the reduction peak of the additional couple. This experiment provided direct evidence the FSCV peaks were Faradaic in nature. Here, we ask whether Ca(II) and Al(III) ions, that are commonly difficult to analyze follow the same phenomenon. The panels in Figure 2A show slow-scan CVs of 1.0 M Ca(II) (left orange panel) and 0.1 M Al(III) (right blue panel) in 0.01 M NaCl for different scan rates (10−100 mV s^{-1}). Here we do not observe the classic nucleation/growth and stripping peaks because they occur outside of our potential window. However, particularly in the case of Ca(II), a small reduction peak at around −0.3 V is seen to shift with increasing scan rate, an indication of Faradaic processes. Figure 2B shows background-subtracted fast scan CVs (50−400 V s^{-1}). Redox peaks are easily captured after background subtraction for these fast scan voltammograms (Figure 2B). The peak width and the peak amplitude both increase as scan rate increases, behavior attributed to adsorbed species and Faradaic processes as we previously described for Cu(II). We can therefore postulate that the unique adsorption driving force of activated carbon fibers enables, for the first time, real-time electrochemical measurements of Ca(II) and Al(III). The redox peaks for these metals are captured within the CFM potential window because adsorption becomes a significant driver in bringing the analyte to the surface, thereby reducing the energy required for voltammetric detection by facilitating electron transfer.

Other examples of metals that are traditionally difficult to rapidly analyze are Mg(II) and Zn(II). Like Ca(II) and Al(III), Mg(II) has a high reduction potential and is thus difficult to analyze. Zn(II) analysis should be possible within the potential window of traditional materials but nucleation/growth processes that underlie preconcentration limit fast analysis.[9] Since CFMs preconcentrate analytes via adsorption, next we investigated whether Mg(II) and Zn(II) also display redox peaks on CFMs.

Characterization of Ca(II), Al(III), Zn(II), and Mg(II). In this experiment, FSCV is performed in a flow injection analysis (FIA) system with various concentration ranges of Ca(II) (0.1−100 mM), Al(III) (1−500 μM), Zn(II) (0.5−500 μM), and Mg(II) (0.1−100 μM). Details of the setup and instrumentation for FIA were described previously.[20] The potential limits, resting potential, and scan rate are all optimized to obtain a CV with a well-defined reduction peak and to provide optimal sensitivity for each species (see Figure 1). Figure 3A shows representative color plots for a square injection of each metal where a reduction event is clearly apparent. Figure 3B shows CVs extracted from the color plots at the position of the dashed vertical lines.

It is difficult to compare the peak positions and currents between the four because of the different waveforms utilized. However, the reduction peaks that appeared at approximately −0.3, −0.4, −0.6, and −0.5 V on the Ca(II), Al(III), Zn(II), and Mg(II) CVs, respectively, can be employed to construct calibration curves (Figure 3C). The linear range and limit of quantitation (LOQ) for each metal were calculated and are tabulated in Table 1. In all cases, the linear range and LOQ are sufficient to perform analysis in a range of physiological and environmental systems.[31−33] Our technique's LOD lies within the range of other methods, summarized in Table 2, even though the analysis is performed on a fundamentally different temporal scale (orders of magnitude faster).

Table 1. Calibration Parameters for Each Metal[a]

metal	linear range	LOQ	LOD
Ca(II)	0.10−5.00 mM	0.1 mM	30 μM
Al(III)	1.00−50.00 μM	1.00 μM	300 nM
Zn(II)	0.50−20.00 μM	0.50 μM	150 nM
Mg(II)	0.010−2.00 mM	0.010 mM	3 μM

[a] We report the limit of quantitation, LOQ, and limit of detection, LOD, for our method.

Table 2. Reported Limit of Detection for the Four Metals via Alternate Methods Compared to FSCV

metal	method	LOD
Ca(II)	potentiometry with ionophores	1 mM[8]
	stripping voltammetry with polymer coating	0.1 nM[21]
	amperometry with polymer coating	0.5 μM[22]
	galvanostatic polarization with ionophore	0.1 nM[23]
	differential pulse voltammetry with Au nanoparticles-modified electrode and chelating agent	0.51 μM[24]
	Ca(II)-imprinted membrane electrode	0.75 μM[25]
	Ca(II)-selective solid state microelectrodes	1 μM[26]
Al(III)	adsorptive stripping voltammetry (Arancibia et al.[7])	1 nM−1.8 μM
Zn(II)	electrochemical biosensors (Gumpu et al.[27])	1.4 nM[28]−100 nM
Mg(II)	potentiometry with ionophores	50 μM[8]
	adsorptive stripping voltammetry	0.31 μM[29]
	square wave adsorptive stripping voltammetry with electroactive ligand	6 nM[30]

The source of metal inherently constitutes an anion. To verify that this anion does not voltammetrically contribute to the signal, the following experiment was performed. Three solutions of Zn(II) were prepared: 250 μM $Zn(NO_3)_2$, a mixture of 125 μM $Zn(NO_3)_2$ and 125 μM $ZnSO_4$, such that the Zn(II) concentration remained the same, and 250 μM $ZnSO_4$. The three responses were identical, showing that the anion does not affect the signal as observed in Figure 4.

Metal Adsorption onto CFMs Is Consistent with Adsorption onto Other Activated Carbon Materials. Once again, it is difficult to compare the thermodynamic properties of the different FSCV signals for each metal because different waveforms are necessary for optimal analysis. However, it is possible to compare adsorption profiles by constructing isotherms and calculating equilibrium constants for metal-CFM adsorption (K_{ads}). We previously reported the adsorption isotherm profile for Cu(II)-CFM, which agrees well with a Langmuir adsorption isotherm, suggesting a monolayer of Cu(II) on CFMs.[13] Here we generate adsorption profiles for our four metals using FSCAV to ask whether Langmuir's theory also applies.

We perform FSCAV experiments for each metal in a simple matrix, NaCl. Although we previously reported that the

DOI: 10.1021/acs.analchem.8b02210
Anal. Chem. 2018, 90, 11917−11924

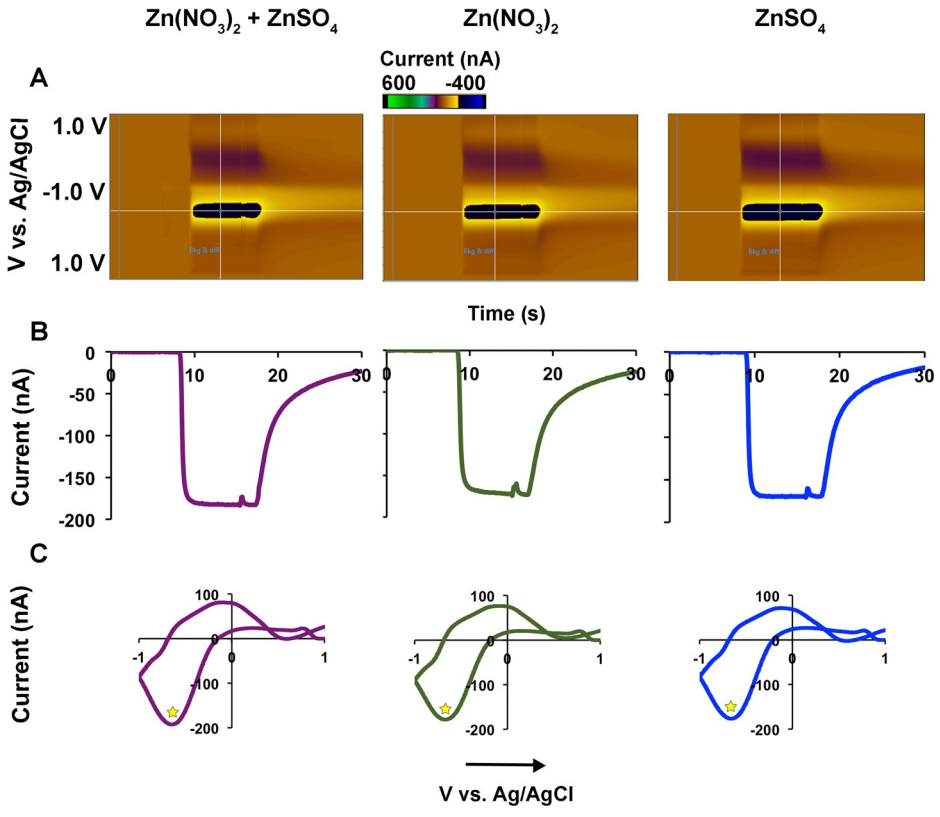

Figure 4. Data for FIA (2 mL min^{-1}) for 125 μM $Zn(NO_3)_2$ + 125 μM $ZnSO_4$, 250 μM $Zn(NO_3)_2$, and 250 μM $ZnSO_4$. The Zn(II) concentration is the same across all three solutions. (A) 2D color plot showing potential sweep on the y-axis and time (in s) on the x-axis. The color indicates t in nA. The black plug indicates a 10-s bolus injected into the flow cell. A horizontal cross section through the bolus injection generates the cu time curve shown in part B while a vertical cross section through the bolus injection generates the current vs potential cyclic voltammograms part C. The peak indicated by the star is the reduction peak for Zn(II) and its magnitude is not affected by the nature or concentration anion us (NO_3^- or SO_4^{2-}).

surrounding matrix does not significantly disturb Cu(II) adsorption on CFMs,[20] it is best to use a matrix without competing equilibria to simplify the experiment. A series of different concentrations of each metal (Figure 5A−D) was prepared in 0.01 M NaCl and the surface concentration of each metal was calculated as explained above.[13] The experimental data fit well to a linearized Langmuir model as shown in Figure 5ii, confirming monolayer adsorption. K_{ads} for each metal was calculated using eq 1. Figure 5iii represents a schematic diagram that illustrates the adsorption equilibrium and K_{ads} of each metal onto the CFM.

Adsorption favorability of these four metals to CFMs is evaluated by comparing the adsorption constants we obtain to those reported in the literature for these metals onto other activated carbon materials. Since our carbon fibers are activated electrochemically by oxidizing at 1.3 V prior to each experiment, we hypothesize the order of adsorption should be similar for these four metals as on activated carbon materials that are used to "remove" metals from aqueous systems. Alkali earth metals adsorb weakly onto activated carbon[34] and our data support this since Mg(II) has the lowest adsorption constant onto CFMs followed by Ca(II). We previously studied Cu(II) adsorption[13] and reported the K_{ads} value as 4.12×10^{9}, and we report here the K_{ads} of Zn(II) is lower than that of Cu(II) at 5.95×10^{8}.

Literature validates this result, showing that Cu(II) adsorption is more favorable than Zn(II) onto carbon.[35,36] Comparison of Al(III) adsorption to other metals has not been reported in the literature. Here we report that Al(III) has a similar adsorption to Cu(II) on carbon fibers. In summary, we report increasing adsorption trends as thus: Mg(II) < Ca(II) < Zn((II) < Al(III) ≤ Cu(II)).

Our results provide evidence that small metal ions follow monolayer adsorption onto CFMs and have different adsorption efficiencies based on their size and electrostatic interactions with carbon fibers. In these four cases, it is also clear that the kinetics of adsorption are rapid enough such that a 100 ms rest time between scans is sufficient for preconcentration. We next apply this method to tracking the levels of these four metals in real time using metal chelators.

Real-Time Trace Metal Complexation. As proof of principle that the levels of these four metals can be tracked in real time, we perform dynamic complexation studies. It is important to note that, as it stands, this method would not be useful to study real or complex samples due to selectivity issues. We have created ultraselective Cu(II) electrodes via modification of the CFM surface with Cu(II) selective ionophores[37] and plan to apply to same strategy here for future analysis. Nonetheless, the method is able to look at real-time complexation of our four metals in a simple matrix as proof of concept.

In these experiments, EDTA and BAPTA are utilized as ligands with varying affinities for the four metals. BAPTA has been shown to selectively bind to Ca(II), in a mixture of Ca(II) and Mg(II), serving as a selective chelator for Ca(II) in biological matrixes. However, BAPTA does have affinity for other divalent cations such as Zn(II).[38] EDTA is chosen as a universal chelator as it binds nonselectively to most metals. The

DOI: 10.1021/acs.analchem.8b02210
Anal. Chem. 2018, 90, 11917−11924

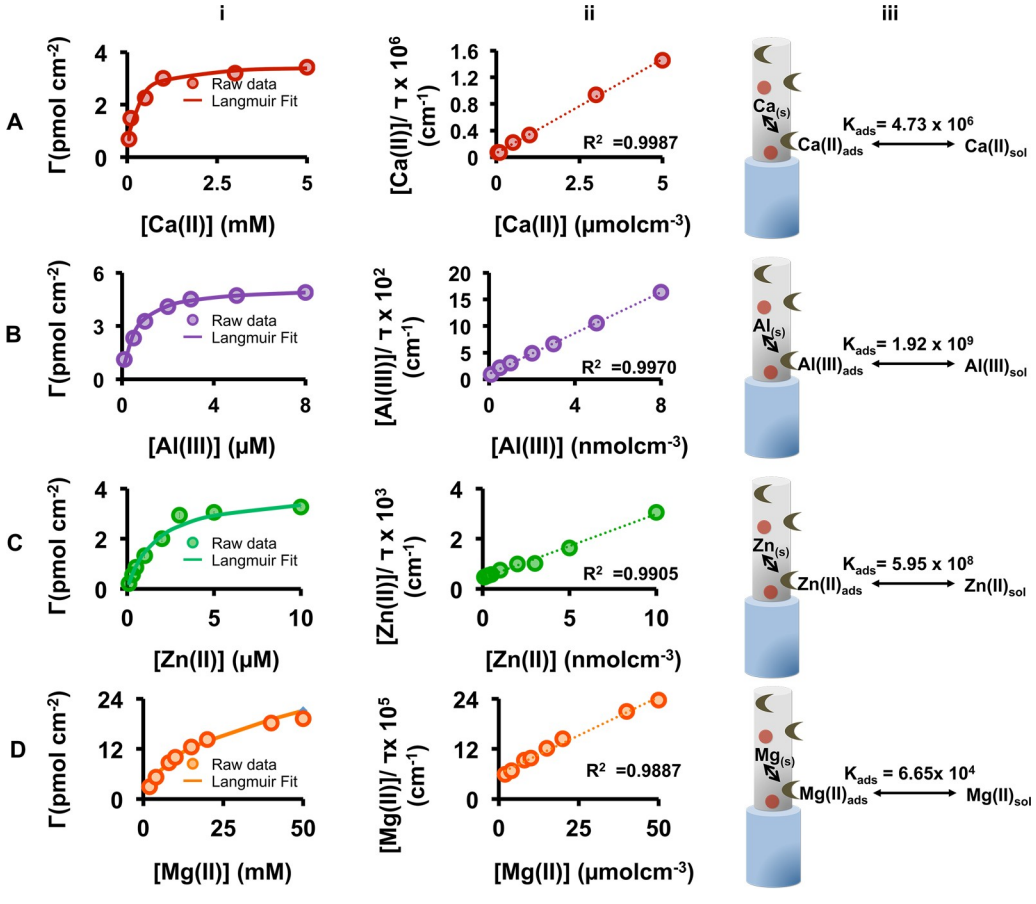

Figure 5. Adsorption profiles for (A) Ca(II), (B) Al(III), (C) Zn(II), and (D) Mg(II). (i) Langmuir isotherm fit with raw data, (ii) linearized Langmuir isotherm, and (iii) schematic representation of solution equilibria near the electrode surface.

experimental paradigm utilized here comprises three steps. Using Ca(II) as an example, the electrode is placed into a stirring solution of 0.01 M NaCl and is allowed to equilibrate. The solid red line on Figure 6A illustrates the change in free Ca(II) concentration over time. After 5 s, Ca(II) is injected into this solution to reach a final concentration of 5 mM. Next, two similar experiments are performed where Ca(II) is spiked into a solution of 2.5 mM BAPTA (dashed red line) and EDTA (dotted red line), respectively. This procedure is repeated for Al(III), Zn(II), and Mg(II) to generate real-time concentration curves (Figure 6C,D). Different concentrations are used depending on the linear range and environmental availability (see Table 1 and methods).

When the metals are injected into EDTA solution, as expected, since EDTA has affinity for all four metals, there is a decrease in free concentration of these metals and thus a lower signal. The largest effect can be seen with Zn(II) and Al(III) (log K_f of metal-EDTA binding = 16.5 and 16.13, respectively[39]) where the metal concentration is reduced by approximately 41 and 31%, respectively. There is a lesser effect for Ca(II) and Mg(II) (reflected in the lower log K_f of metal-EDTA binding values of 10.96 and 8.69, respectively[39]) whose concentrations are reduced by 20−26%. When injected into BAPTA, however, the largest effects are seen with Zn(II) and Ca(II) (decrease in concentration of these metals by approximately 23 and 20%, respectively) but much smaller effects are observed for Mg(II) and Al(III) (change in concentration of free metal ions by around 6 and 2%, respectively). This is consistent with the decreasing trend in the log K as follows: Zn(II)-BAPTA (log K = 9.38) > Ca(II)-BAPTA (log K = 6.97) > Mg(II)-BAPTA (log K = 1.77).[39] To the best of our knowledge, the log K has not been reported for Al(III)-BAPTA presumably because it is negligibly small.

To this end, a linear regression can fit the relationship between log K and % change in concentration after BAPTA and EDTA binding (Figure 7) with a slope of 2.3 ± 0.1 (±SEM, y-axis errors bars are present but are smaller than the markers). We use this correlation to estimate the log K value for the Al(III)-BAPTA binding to be 0.82 ± 0.05 (±SEM).

Real-time monitoring of ligand affinities has implications in both biological and environmental applications. The above complexation measurements are proof-of-principle demonstrations that our method can not only monitor real-time binding between trace metal ions and chelators but is also sensitive to different binding affinities. This real-time monitoring of metal−ligand complexation, to the best of our knowledge, has never been done before electrochemically. Other electrochemical methods do not have the temporal resolution required to perform these analyses.

CONCLUSION

In this manuscript, we demonstrated that metals traditionally difficult to electroanalyze, due to negative standard reduction potentials (in the cases of Ca(II), Al(III), and Mg(II)) and the need for nucleation and growth (in the case of Zn(II)), could be rapidly analyzed using CFMs with FSCV. We measured FSCV reduction peaks for these four metals and demonstrated that the adsorption profiles of these metals onto CFMs follow Langmuir

DOI: 10.1021/acs.analchem.8b02210
Anal. Chem. 2018, 90, 11917−11924

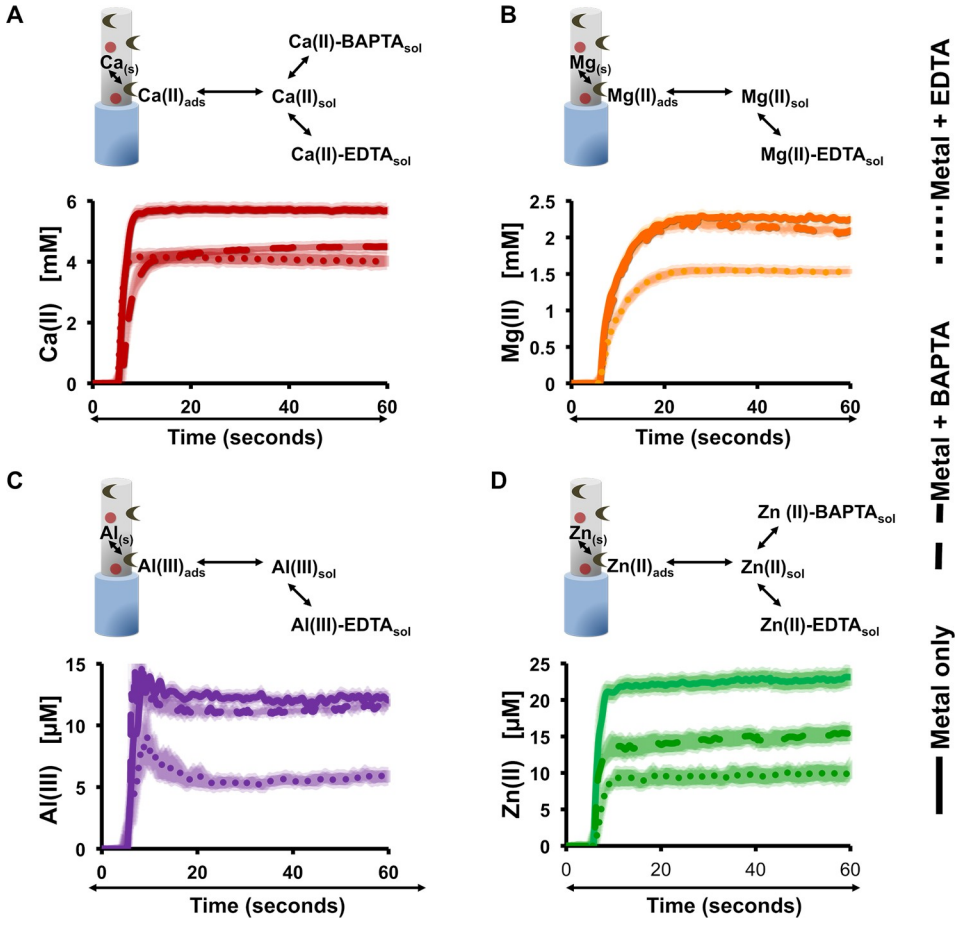

Figure 6.Schematic representation of different equilibria in each solution (solid line) and real-time complexation data with EDTA (dotted) and BAPTA (dashed) for (A) Ca(II), (B) Mg(II), (C) Al(III), and (D) Zn(II). The shaded area around each line represents the standard error of mean (SEM) for a total of 12 repetitions.

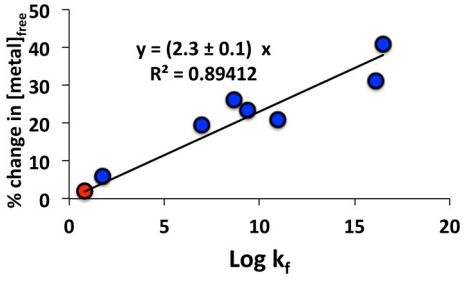

Figure 7. Correlation plot between the% change in free metal ($[metal]_{free}$) ion concentration as a function of the formation constant($\log k_f$). The red dot indicate the extrapolated point for Al(III)-BAPTA binding.

monolayer isotherms. Calculated K_{ads} values of metal adsorption onto CFMs were consistent with those previously reported for other activated carbon materials. Finally, a real-time complexation study using metal chelators BAPTA and EDTA illustrate the selectivity of the signals and ability of the method to differentiate between metal−chelator formation constants. We also observed a linear relationship between the % change in free [metal] and the $\log k_f$. We fit a linear regression to this relationship and extrapolated a $\log k_f$ estimate for Al(III)-BAPTA binding to be 0.82 ± 0.05 (±SEM). To the best of our knowledge, this is the first report of the formation constant for this complex. Taken together, this work established the capacity of FSCV as a method to extend the reach of rapid electroanalysis.

AUTHOR INFORMATION

Corresponding Author
*E-mail: hashemi@mailbox.sc.edu. Phone: (803) 777-6104. Fax: (803) 777-9521.
ORCID
Pavithra Pathiratna: 0000-0001-9222-9109
Parastoo Hashemi: 0000-0002-0180-767X

Notes
The authors declare no competing financial interest.

ACKNOWLEDGMENTS

The authors would like to thank Campbell Mousseau and Navid Tavakoli for experimental assistance and Rachel Saylor for helpful comments. NSF CAREER Award CHE-1654111 (P.H.) funded this work.

REFERENCES

(1) Tchounwou, P. B.; Yedjou, C. G.; Patlolla, A. K.; Sutton, D. J. In Molecular, Clinical and Environmental Toxicology; Springer, 2012; pp 133−164.
(2) Dorne, J. L.; Kass, G. E.; Bordajandi, L. R.; Amzal, B.; Bertelsen, U.; Castoldi, A. F.; Heppner, C.; Eskola, M.; Fabiansson, S.; Ferrari, P. Met. Ions Life Sci. 2011, 8, 27−60.
(3) Jarup, L. Br. Med. Bull. 2003, 68, 167−182.

DOI: 10.1021/acs.analchem.8b02210
Anal. Chem. 2018, 90, 11917−11924

(4) Economou, A. TrAC, Trends Anal. Chem. 2005, 24, 334−340.
(5) Zhang, F.; Bi, S.; Zhang, J.; Bian, N.; Liu, F.; Yang, Y. Analyst 2000, 125, 1299−1302.
(6) Wang, J.; Farias, P. A. M.; Mahmoud, J. S. Anal. Chim. Acta 1985, 172, 57−64.
(7) Arancibia, V.; Munoz, C. Talanta 2007, 73, 546−552.
(8) Zhu, J.; Qin, Y.; Zhang, Y. Anal. Chem. 2010, 82, 436−440.
(9) Andersen, J. E. T. Anal. Lett. 1997, 30, 1001−1012.
(10) Wang, J. Electroanalysis 2005, 17, 1341−1346.
(11) Pathirathna, P.; Yang, Y.; Forzley, K.; McElmurry, S. P.; Hashemi, P. Anal. Chem. 2012, 84, 6298−6302.
(12) Yang, Y.; Pathirathna, P.; Siriwardhane, T.; McElmurry, S. P.; Hashemi, P. Anal. Chem. 2013, 85, 7535−7541.
(13) Pathirathna, P.; Samaranayake, S.; Atcherley, C. W.; Parent, K. L.; Heien, M. L.; McElmurry, S. P.; Hashemi, P. Analyst 2014, 139, 4673−4680.
(14) Rousset, M.; Cens, T.; Vanmau, N.; Charnet, P. FEBS Lett. 2004, 576, 41−45.
(15) Mantoura, R. F. C.; Dickson, A.; Riley, J. P. Estuarine Coastal Mar. Sci. 1978, 6, 387−408.
(16) Sillanpää, M.; Oikari, A. Chemosphere 1996, 32, 1485−1497.
(17) Atcherley, C. W.; Laude, N. D.; Parent, K. L.; Heien, M. L. Langmuir 2013, 29, 14885−14892.
(18) Abdalla, A.; Atcherley, C. W.; Pathirathna, P.; Samaranayake, S.; Qiang, B.; Peña, E.; Morgan, S. L.; Heien, M. L.; Hashemi, P. Anal. Chem. 2017, 89, 9703−9711.
(19) Liu, Y.; Xu, L. Sensors 2007, 7, 2446−2457.
(20) Pathirathna, P.; Siriwardhane, T.; McElmurry, S. P.; Morgan, S. L.; Hashemi, P. Analyst 2016, 141, 6432−6437.
(21) Kabagambe, B.; Garada, M. B.; Ishimatsu, R.; Amemiya, S. Anal. Chem. 2014, 86, 7939−7946.
(22) Hurrell, H. C.; Abruna, H. D. Anal. Chem. 1988, 60, 254−258.
(23) Peshkova, M. A.; Sokalski, T.; Mikhelson, K. N.; Lewenstam, A. Anal. Chem. 2008, 80, 9181−9187.
(24) Yang, J.-X.; He, Y.-B.; Lai, L.-N.; Li, J.-B.; Song, X.-L. Biosens. Bioelectron. 2015, 66, 417−422.
(25) Alizadeh, T.; Shamkhali, A. N.; Hanifehpour, Y.; Joo, S. W. New J. Chem. 2016, 40, 8479−8487.
(26) Ummadi, J. G.; Downs, C. J.; Joshi, V. S.; Ferracane, J. L.; Koley, D. Anal. Chem. 2016, 88, 3218−3226.
(27) Gumpu, M. B.; Sethuraman, S.; Krishnan, U. M.; Rayappan, J. B. B. Sens. Actuators, B 2015, 213, 515−533.
(28) Chaiyo, S.; Mehmeti, E.; Žagar, K.; Siangproh, W.; Chailapakul, O.; Kalcher, K. Anal. Chim. Acta 2016, 918, 26−34.
(29) Zezza, T. R. C.; Paim, L. L.; Stradiotto, N. R. Int. J. Electrochem. Sci. 2013, 8, 658−669.
(30) Farghaly, O. A. Talanta 2004, 63, 497−501.
(31) Nagajyoti, P. C.; Lee, K. D.; Sreekanth, T. V. M. Environ. Chem. Lett. 2010, 8, 199−216.
(32) Crapper, D. R.; Krishnan, S. S.; Dalton, A. J. Science 1973, 180, 511−513.
(33) Parisi, A. F.; Vallee, B. L. Am. J. Clin. Nutr. 1969, 22, 1222−1239.
(34) Goldin, M. M.; Volkov, A. G.; Namychkin, D. N.; Filatova, E. A.; Revina, A. A. J. Electrochem. Soc. 2005, 152, E172−E175.
(35) Bouhamed, F.; Elouear, Z.; Bouzid, J.; Ouddane, B. Environ. Sci. Pollut. Res. 2016, 23, 15801−15806.
(36) Stafiej, A.; Pyrzynska, K. Sep. Purif. Technol. 2007, 58, 49−52.
(37) Yang, Y.; Ibrahim, A. A.; Hashemi, P.; Stockdill, J. L. Anal. Chem. 2016, 88, 6962−6966.
(38) Csermely, P.; Sándor, P.; Radics, L.; Somogyi, J. Biochem. Biophys. Res. Commun. 1989, 165, 838−844.
(39) Dojindo Molecular Technologies Inc. Metal Chelates; Washington, DC, 2012; pp 252−253.

DOI: 10.1021/acs.analchem.8b02210
Anal. Chem. 2018, 90, 11917−11924